Example. Typical timing parameters for T2 weighted SE imaging are TR ~ 2 sec and TE ~ 75 msec, leading to an 8.5 min scan time for N_y=256. The scan time can be shortened substantially using the fast spin echo sampling method (Chapter 7, Fig.7.13c) T2 weighted images are routinely acquired in clinical protocols to visualize inflammation, edema, or hypervasculature, which all decrease cellular contents ($\propto 1/T2$) in a voxel through membrane breakdown and cellular content leakage.

$ 3.2.4 Echo formation from n RFs: magnetization evolution and phase graph

The phase-tracing analysis in Fig.3.12 can be applied to study many echo formations when three or more RF pulses are applied to a spin system. As we may expect, every pair of RF pulses can generate a spin echo. Furthermore, there are other echoes in addition to these spin echoes. A spin echo itself can be mirrored by an RF pulse to generate an indirect spin echo. The phase evolution between a pair of two RF pulses can be preserved in the z-component, dissipating at time constant T1 (≫T2*) and unlocked by flipping into the transverse plane using a third RF pulse to generate a stimulated echo. These echo formations can be nicely organized according to the phase evolution pathways under an inhomogeneous field.

Magnetization evolution and phase graph

The full solution to the Bloch equation can be represented by an evolution matrix that transforms an initial spin vector into a spin vector at a current time. The evolution matrix integrates the effects of RF fields, gradient fields, and tissue inhomogeneity fields acting on the spin vector and relaxation effects over the time course. The evolution matrix can be decomposed into a multiplication of rotation matrices for all magnetic field effects and relaxation matrices. This evolution matrix approach to studying the Bloch equation provides a rigorous justification for the small angle approximation description of the RF excitation process discussed in Chapter 2. More importantly for the pulse sequence design, symmetry in the rotation matrices allows the formation of various spin echoes, including the so-called superechoes under a special design of RF trains.

The above statements can be derived from Eq.3.13, which can be solved by dividing and conquering. We review here the basic effects of RF and Larmor precession using systematic linear matrix algebra. Fig.3.15 illustrates a) an RF pulse with a flip angle α and field $\mathscr{b}_1$ along the Y- axis, which rotates and mixes the X, Z components, and b) Larmor precession under a local field b.

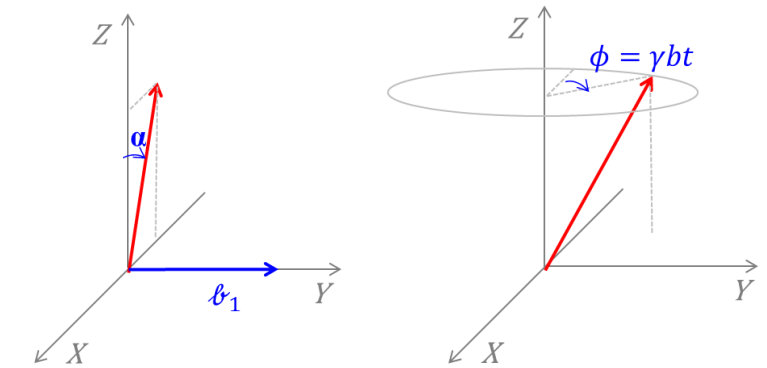

Fig.3.15. a) An α RF pulse with $\mathscr{b}_1$ along the Y- axis rotates and mixes the XZ components of an isochromat. b) The inhomogeneous local field at the location of the isochromat makes the isochromat precess, accumulating a phase ϕ.

Let the magnetization immediately before the RF be m', and immediately after the RF be m (Fig.3.15a). Then we have the following expressions of magnetization component changes ($m_\perp = m_x + im_y$):

$$\begin{bmatrix} m_x \\ m_y \\ m_z \end{bmatrix} = \begin{bmatrix} \cos\alpha & 0 & -\sin\alpha \\ 0 & 1 & 0 \\ \sin\alpha & 0 & \cos\alpha \end{bmatrix} \begin{bmatrix} m'_x \\ m'_y \\ m'_z \end{bmatrix} \qquad [3.39]$$

$$m_\perp = \cos^2\frac{\alpha}{2} m'_\perp - \sin^2\frac{\alpha}{2} m'^*_\perp - \sin\alpha\, m'_z$$

$$m_z = \frac{1}{2}\sin\alpha\, m'_\perp + \frac{1}{2}\sin\alpha\, m'^*_\perp + \cos\alpha\, m'_z \qquad [3.39a]$$

After RF excitation, a local field b (always along the Z direction) rotates and mixes the XY components (Larmor precession, Fig.3.15b):

$$\begin{bmatrix} m_x \\ m_y \\ m_z \end{bmatrix} = \begin{bmatrix} \cos\phi & \sin\phi & 0 \\ -\sin\phi & \cos\phi & 0 \\ 0 & 0 & 1 \end{bmatrix} \begin{bmatrix} m'_x \\ m'_y \\ m'_z \end{bmatrix} \qquad [3.40]$$

$$m_\perp = e^{-i\phi} m'_\perp, \qquad m_z = m'_z \qquad [3.40a]$$

Using Eq.3.14 to account for relaxation effects and the above Eqs.3.39-40a, we can examine the state of magnetization between two successive RFs α_{n-1} and α_n as illustrated in Fig.3.16. The RF pulse durations (~1 msec) are much shorter than the time separation between two pulses (~10 msec), and the RF fields ($\mathscr{b}_1$) are much stronger than an inhomogeneous local field (b) and

relaxation rates ($\gamma b_1 \gg \gamma b, \gamma b_1 \gg \frac{1}{T2} > \frac{1}{T1}$). So we only need to consider the effects of the inhomogeneous field (phase accumulation $\phi_{n-1} = \gamma b \tau_{n-1}$) and relaxation (transverse decay $e^{-\frac{\tau_{n-1}}{T2}}$ and longitudinal regrow $\left(1 - e^{-\frac{\tau_{n-1}}{T1}}\right) + e^{-\frac{\tau_{n-1}}{T1}} m_{z,n-1} \equiv R_n$) in the duration between RF pulses. Because the relaxation effects do not rotate/mix the magnetization components (characterized by a diagonal matrix), the magnetization evolution from that immediately after the $(n+1)^{\text{th}}$ RF (m_{n-1}) to that immediately after the n^{th} RF (m_n) can be written by combining Eqs.40a&14 into Eq.39a (all RFs are Y- axis):

$$\begin{aligned} m_{\perp,n} = {} & e^{-i\phi_{n-1}} e^{-\frac{\tau_{n-1}}{T2}} \cos^2\frac{\alpha_n}{2} m_{\perp,n-1} \\ & + e^{i\phi_{n-1}} e^{-\frac{\tau_{n-1}}{T2}} \left(-\sin^2\frac{\alpha_n}{2}\right) m_{\perp,n-1}{}^* \\ & + (-\sin\alpha_n)\left(\left(1 - e^{-\frac{\tau_{n-1}}{T1}}\right) + e^{-\frac{\tau_{n-1}}{T1}} m_{z,n-1}\right) \end{aligned} \quad [3.41]$$

$$\begin{aligned} m_{z,n} = {} & e^{-i\phi_{n-1}} e^{-\frac{\tau_{n-1}}{T2}} \left(\frac{1}{2}\sin\alpha_n\right) m_{\perp,n-1} \\ & + e^{i\phi_{n-1}} e^{-\frac{\tau_{n-1}}{T2}} \left(\frac{1}{2}\sin\alpha_n\right) m_{\perp,n-1}{}^* \\ & + (\cos\alpha_n)\left(\left(1 - e^{-\frac{\tau_{n-1}}{T1}}\right) + e^{-\frac{\tau_{n-1}}{T1}} m_{z,n-1}\right) \end{aligned} \quad [3.42]$$

These solutions state that the magnetization evolution from the (n-1)th RF to the nth RF involves three phase pathways, $\phi_{n-1}, 0, -\phi_{n-1}$, which are mixed by each RF. Whenever there is a negative phase, there will be an echo at phase nulling in the standard detection of the clockwise precession component, as illustrated in Fig.3.12 for spin echo formation. Accordingly, the phase pathways from Eqs.3.41&42 can be traced as tree structures to depict echo formation from multiple RF pulses (Fig.3.16), which is called phase graph. Immediately after the 2nd RF, there is only one negative phase $-\phi_1$ allowing formation of one echo (echo at time $2\tau_1$ in Fig.3.16, as the standard spin echo in Fig.3.13). The 3rd RF introduces four additional negative phases, $-(\phi_2 - \phi_1), -\phi_1, -\phi_2, -(\phi_2 + \phi_1)$, allowing the formation of 4 additional echoes (Fig.3.16) at times: $2\tau_2, 2\tau_1 + \tau_2, \tau_1 + 2\tau_2, 2(\tau_1 + \tau_2)$. The echo at time $2\tau_1 + \tau_2$ is referred as the stimulated echo and it does not involve phase accumulation from the 2nd RF to the 3rd RF.

Example. The maximal number of distinct phases after the nth RF is $P_n = 2\sum_{i=1}^{n-1} P_i + 1$ according to the 3 pathways in Fig.3.16. $P_1 = 1,\ P_2 = 3, \ldots,\ P_n = 3^{n-1}$. Proof: If $P_{n-1} = 3^{n-2}$, then $P_n = 2\sum_{i=1}^{n-1} 3^{i-1} + 1 = 2(3^{n-1} - 1)/(3-1) + 1 = 3^{n-1}$. The maximal number of negative phases or echoes is $(P_n - 1)/2 = (3^{n-1} - 1)/2$.

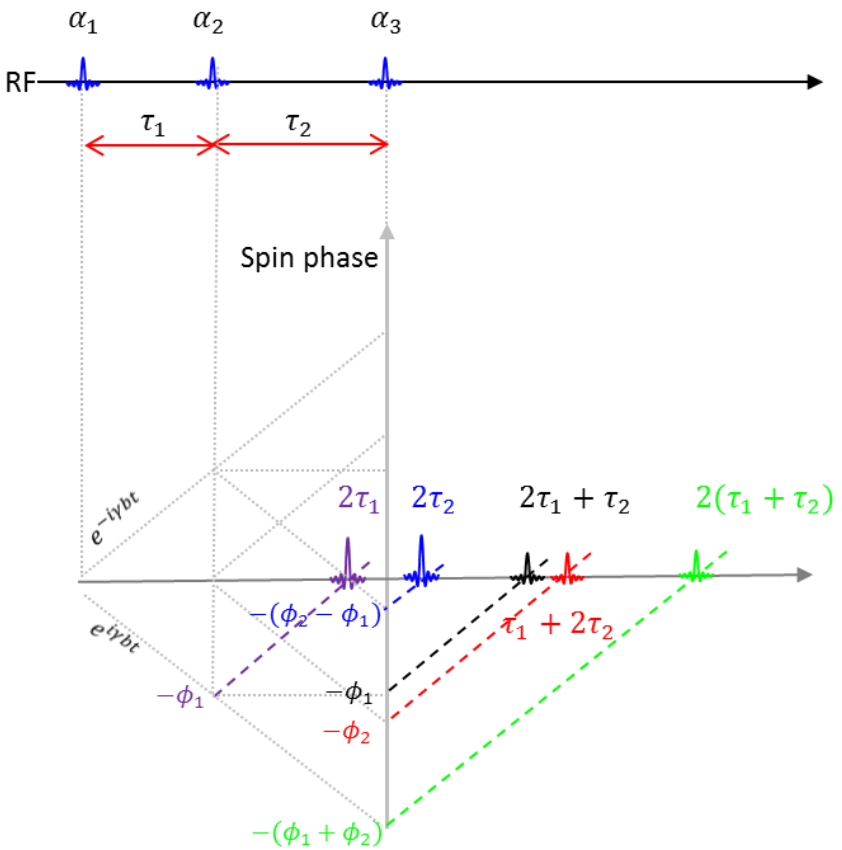

Fig.3.16. Phase graphs for echo generation. Magnetization evolution from the (n-1)th RF to the nth RF has 3 phase pathways, $\phi_{n-1}, 0, -\phi_{n-1}$.For a given isochromat, the phase accumulation rate is the same (γb) as indicated by the single absolute slope in the graph. There will be an echo for every negative phase after echo RF.

Weighted phase graph

The echo amplitude can be algebraically calculated by iterating Eqs.3.41&42 over all RFs. This algebra can be systematically organized by adding weights to the edges in the phase graph: an echo amplitude is the multiplication of the edge weights along the phase pathways. The weight assignment is determined by Eqs.3.41&42 (m_0=1) and is illustrated in Fig.3.17a, which exemplifies the spin echo amplitude. The weight at an edge represents the magnetization state immediately after the RF at the edge's end node. A T2 decay factor is added to the final edge (dashed) leading to echo formation. When an edge of zero phase propagation is involved, switching back and forth between $m_\perp$ and m_z may be involved. The amplitudes for all other echoes in Fig.3.16 are illustrated in weighted phase graphs Figs.3.17b-e.

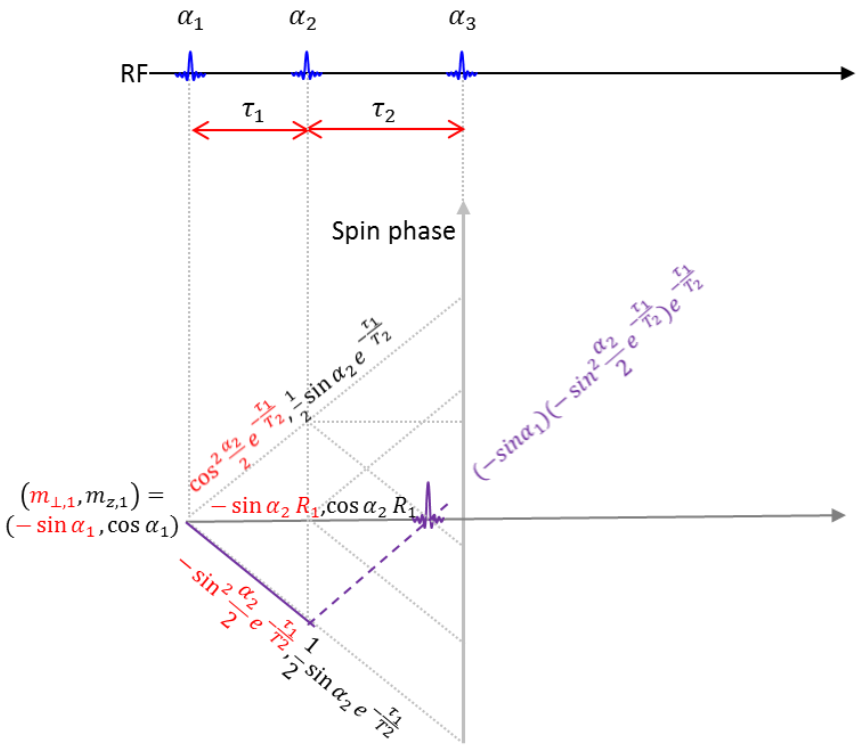

a)

Fig.3.17. Weighted phase graph for amplitude calculation.

- The 1st RF prepares the magnetization state $(m_{\perp,1}, m_{z,1}) = (-\sin\alpha_1, \cos\alpha_1)$.
- The evolution of the transverse magnetization (Eq.3.41) is represented by weights on the three edges (red) with $\cos^2\frac{\alpha_n}{2} e^{-\frac{\tau_{n-1}}{T_2}}$ on the edge of positive phase ϕ_{n-1}, $-\sin^2\frac{\alpha_n}{2} e^{-\frac{\tau_{n-1}}{T_2}}$ on the edge of negative phase $-\phi_{n-1}$, and $(-\sin\alpha_n)\left(\left(1 - e^{-\frac{\tau_{n-1}}{T_1}}\right) + e^{-\frac{\tau_{n-1}}{T_1}} m_{z,n-1}\right) = -\sin\alpha_n R_{n-1}$ on the edge of zero phase.
- The evolution of the longitudinal magnetization (Eq.3.42) is represented by weights on the three edges (black) with $\frac{1}{2}\sin\alpha_n e^{-\frac{\tau_{n-1}}{T_2}}$ on the edge for the positive phase ϕ_{n-1}, $\frac{1}{2}\sin\alpha_n e^{-\frac{\tau_{n-1}}{T_2}}$ on the edge for the negative phase $-\phi_{n-1}$, and $(\cos\alpha_n)\left(\left(1 - e^{-\frac{\tau_{n-1}}{T_1}}\right) + e^{-\frac{\tau_{n-1}}{T_1}} m_{z,n-1}\right) = \cos\alpha_n R_{n-1}$ on the edge of zero phase.
- For the last edge (dashed one) leading to echo formation, its weight is the T2 decay over the edge's temporal length t: $e^{-\frac{t}{T_2}}$.

a) The spin echo from 2 RFs. The 2nd RF encounters the edge $-\phi_1$, which leads to the spin echo indicated by dashed edge that has a weight of $e^{-\frac{\tau_1}{T_2}}$. The product of the initial magnetization, the weight on the edge $-\phi_1$, and the weight on the dashed edge is the echo amplitude: $\sin\alpha_1 \sin^2\frac{\alpha_2}{2} e^{-\frac{2\tau_1}{T_2}}$.

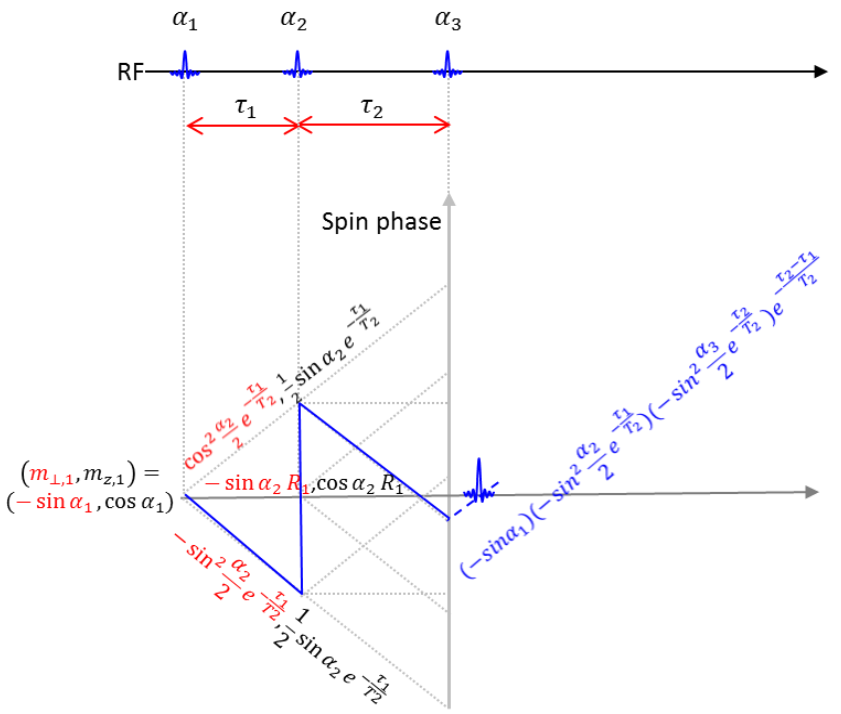

b)

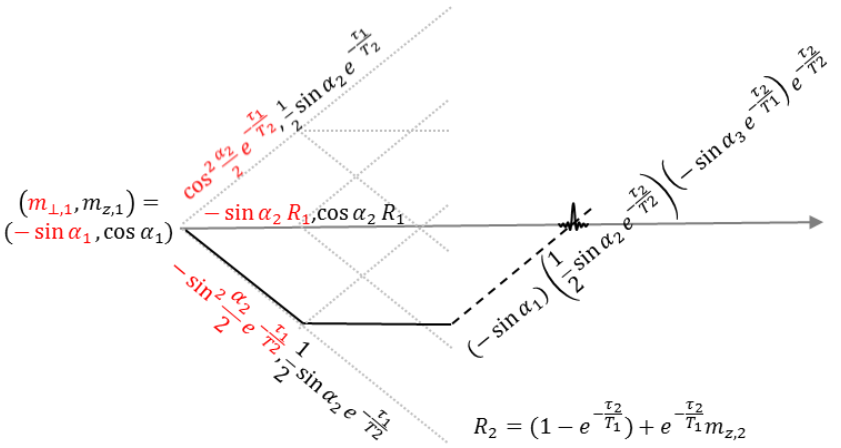

c)

Fig.3.17. b) echo for $-(\phi_2 - \phi_1)$ from 3 RFs. As dictated by Eq.3.41, the negative phase edge is connected to $m_{\perp,n-1}{}^*$, which has an opposite phase evolution from $m_{\perp,n-1}$: $-\sin^2\frac{\alpha_n}{2}e^{-\frac{\tau_{n-1}}{T_2}}$ is weight for the edge of positive phase ϕ_{n-1} in $m_{\perp,n-1}{}^*$. This can be simply represented by a mirrored jump on the weighted phase graph. Then the specific echo amplitude is $-\sin\alpha_1 \sin^2\frac{\alpha_2}{2}\sin^2\frac{\alpha_3}{2}e^{-\frac{2\tau_2}{T_2}}$.

c) stimulated echo for $-\phi_1$ from 3 RFs. The only way to avoid phase accumulation from the 2nd to 3rd RFs is via the zero phase edge in the third term on the right side of Eq.3.41. The m_z evolution from the 2nd to 3rd RFs bridges $m_\perp$'s after the 1st and 3rd RFs . Accordingly, the amplitude is $\frac{1}{2}\sin\alpha_1 \sin\alpha_2 \sin\alpha_3\, e^{-\frac{2\tau_2}{T_2}}e^{-\frac{\tau_2}{T_1}}$.

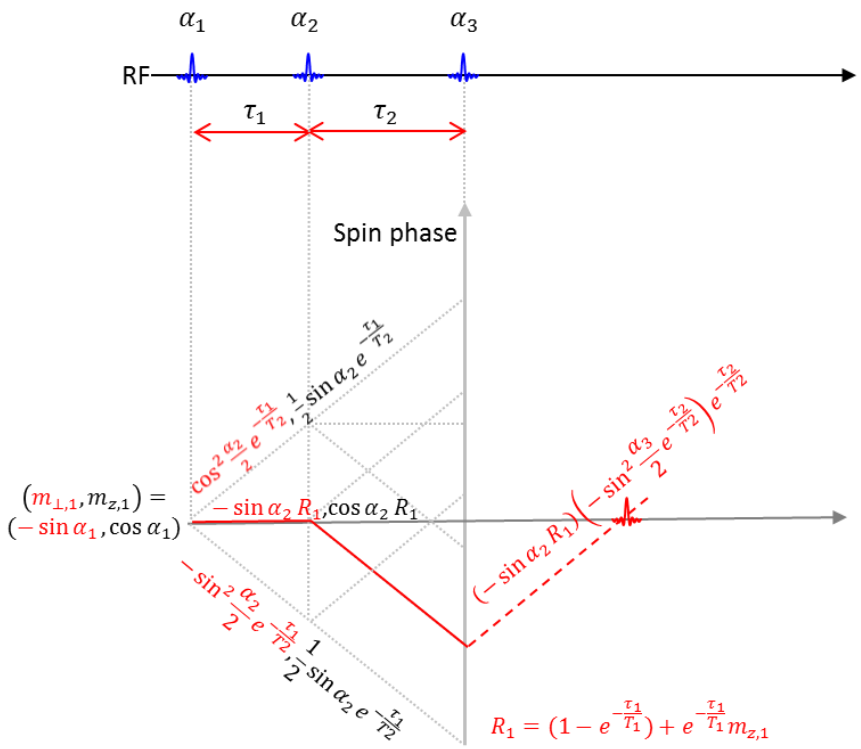

d)

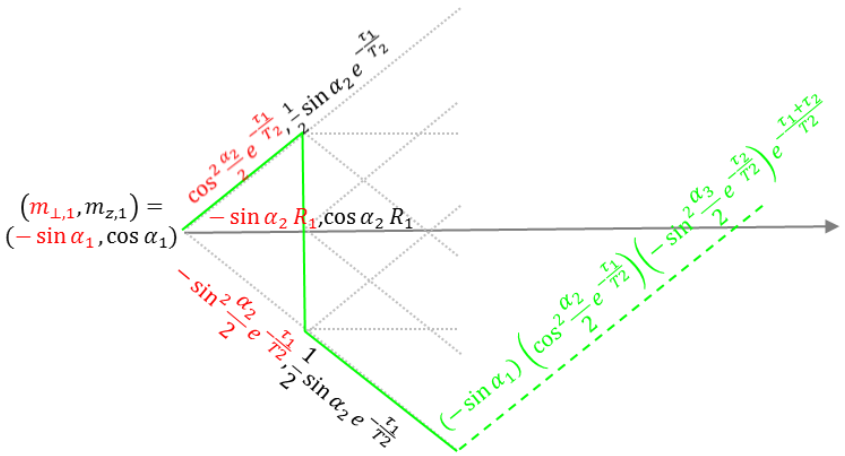

e)

Fig.3.17. d) echo for $-\phi_2$ from 3 RFs. Phase accumulation from the 1st to 2nd RFs is avoided via the zero phase edge that connects to the longitudinal magnetization. Accordingly, the amplitude is $\left(\left(1 - e^{-\frac{\tau_1}{T_1}}\right) + e^{-\frac{\tau_1}{T_1}} \cos\alpha_1\right) \sin\alpha_2 \sin^2\frac{\alpha_3}{2} e^{-\frac{2\tau_2}{T_2}}$.

e) echo for $-(\phi_2 + \phi_1)$ from 3 RFs. As dictated by Eq.3.41, the negative phase $-\phi_2$ edge is connected to $m_{\perp,2}{}^*$ similar to b). Then the specific echo amplitude is $-\sin\alpha_1 \cos^2\frac{\alpha_2}{2} \sin^2\frac{\alpha_3}{2} e^{-\frac{2(\tau_1+\tau_2)}{T_2}}$.